Japanese Journal of Applied Physics

The Japan Society of Applied Physics

ACCEPTED MANUSCRIPT

Characteristics of electron injection at the oxide electrode / polyethylenimine ethoxylated / Alq₃ interface

To cite this article before publication: Masahiro Morimoto *et al* 2019 *Jpn. J. Appl. Phys.* in press https://doi.org/10.7567/1347-4065/ab51e2

Characteristics of Electron Injection at the Oxide Electrode / Polyethylenimine Ethoxylated / Alq_3 Interface

Masahiro Morimoto*, Taishi Yoshida, Shigeki Naka, and Hiroyuki Okada
Graduate School of Science and Engineering for Research, University of Toyama, 3190 Gofuku, Toyama, 930-8555, Japan.
*E-mail: morimoto@eng.u-toyama.ac.jp

Abstract

Inverted organic light-emitting diodes (inverted OLEDs) require electron injection to an organic semiconductor from a transparent oxide electrode. Polyethylenimine ethoxylated (PEIE) has attracted considerable attention as an electron injection material. An injection mechanism has been suggested; however, the barrier height of electron injection has not been determined. In this paper, we present the experimental values for the electron injection barrier height at the transparent oxide electrode/PEIE/organic semiconductor interface. Electron-only devices, consisting of indium-tin-oxide (ITO)/PEIE/tris(8-hydroxyquinolinato) aluminum (Alq_3)/Al, are fabricated. The temperature dependence of the current–voltage curves is measured corresponding to the electron injection of the ITO/PEIE/Alq_3 interface. The current–voltage curves are found to be independent of the measurement temperature, which is explained by the tunneling model. The tunneling injection barriers height are calculated, and the experimental injection barrier height will be important for the development of inverted OLED devices.

1. Introduction

An organic light-emitting diode (OLED)[1,2] generally consists of an oxide electrode having a high work function and a metal electrode having a low work function. Low work function metals, such as Al[3,4] and Ag[25], have been known to cause degradation of device performance due to the oxygen and moisture in the atmosphere. An inverted OLED avoids the degradation of device performance because it consists of a transparent oxide electrode as the cathode, and a metal electrode consisting of a high work-function metal, such as Au or Pt, as the anode[6–8]. The inverted OLEDs have atmospheric stability and favorable hole injection to p-type organic semiconductors. On the other hand, it is difficult to inject electrons from the oxide electrodes to n-type semiconductors; thus, the drive voltage of OLEDs tends to increase with an electrode of high work function because the difference with the lowest unoccupied molecular orbital of organic semiconductors is high.

To improve the device performance and decrease the drive voltage, electron injection layers have been used at the interface of oxide electrodes and organic semiconductors. Several materials have been used, for example, thin metal oxides[9–12] and cationic polymer thin films; however, the mechanisms for these materials are different. The metal oxide layers were used as the buffer layers at the interface of the oxide electrode and organic semiconductor due to the sufficient work function levels and high charge mobility. On the other hand, cationic polymers[13–16] such as polyethyleneimine (PEI) and polyethylenimine ethoxylated (PEIE) are also of interest. These polymers have been reported to decrease the work function of oxide electrodes and to maintain the transmittance of the devices owing to their ultra-thin films. The thin polymer layers do not affect the device structure and the fabrication process; thus, they have been used for OLEDs and organic solar cells[17–19]. An injection mechanism from the PEI or PEIE layers has been suggested in which the work function of oxide electrodes decreases[16,20,21] and the cationic polymers form a high dipole moment on the oxide electrode surface[13,14,22]. It has been reported that the injection layers with PEI or PEIE improved the device performance, such as high luminescence and low voltage drive; however, the barrier height of the electron injection has not been determined.

The carrier injection barrier height at the metal electrode interface has been previously reported[23–25]. The mechanism for the metal/metal interface is explained by the ohmic models, and for the mechanism of the metal/organic interface, Schottky (thermionic)

emission and tunneling models have been suggested. In our previous studies, the carrier injection barrier height was experimentally calculated for the hole injection at the metal oxide/organic interface[12,24] and for the electron injection at the metal/organic interface[23,25]. In this study, we estimate the electron injection barrier height at the oxide electrode/PEIE/organic semiconductor interface using electron-only devices. This mechanism can be explained with the tunneling model because the injection current is independent of the measurement temperature. Furthermore, we reveal one of the important basis properties of inverted OLEDs.

2. Experimental methods

The electron injection layer used in this study is PEIE (Sigma Aldrich). PEIE water-solution was diluted by a factor of 10 using ethanol, and spin-coated at 3000 rpm for 60 s onto indium-tin-oxide (ITO) coated glass substrates. The ITO substrates were treated by ultrasonic cleaning and UV-ozone before the film coating. The PEIE thickness was controlled to be under a few nanometers by the rinse method. Subsequently, 50–150 nm of tris(8-hydroxyquinolinato) aluminum (Alq_3; Lumtec) and 70 nm of Al top electrode were vacuum evaporated. The device structure was ITO/PEIE/Alq_3/Al, which behaved as an electron-only device. The forward bias in this work was determined by ITO, which applied a positive voltage, and Al, which applied a negative voltage. The active area was 2 × 2 mm^2. The photocurrent of the electron-only-devices was measured at 20–30°C under an atmosphere with illumination. The light source measurement was a solar simulator (San-Ei Electric XES-40S3) at a light intensity of 100 mW/cm^2.To evaluate the characteristics of electron injection, the temperature dependence of current density versus applied voltage (*J-V*) curves were measured at 193–293 K under a vacuum using a semiconductor parameter analyzer (Keysight B1500).

3. Results and discussion

Figure 1a shows the magnification of *J-V* curves at low voltage with the 100 nm Alq_3 devices under the illumination of 100 mW/cm^2. The current density under the illumination

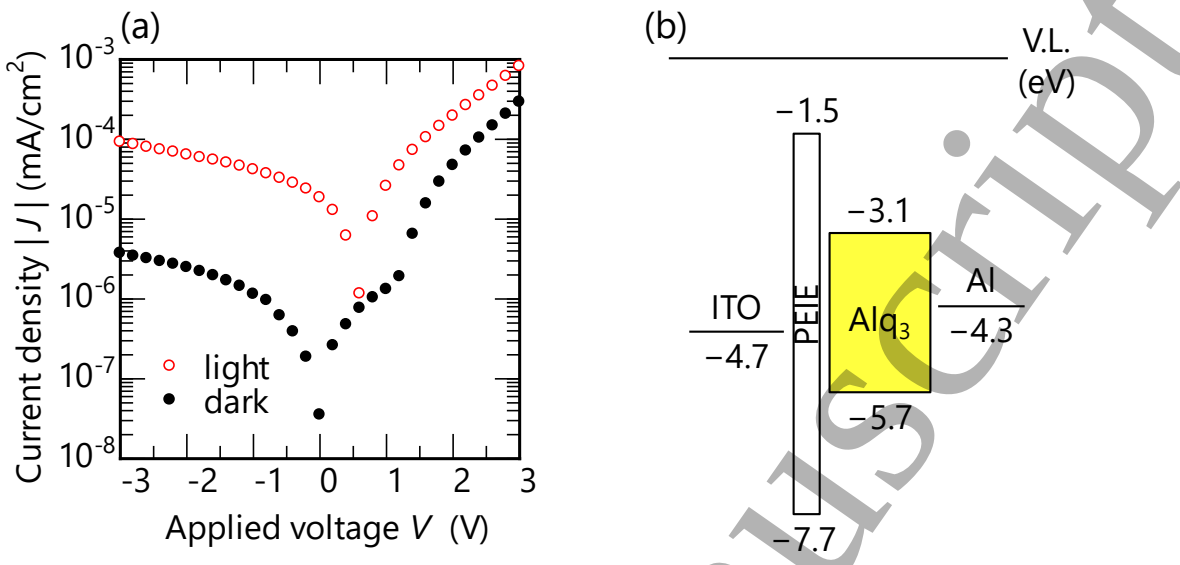

FIG. 1. a) *J-V* curves of the 100 nm Alq_3 device under illumination of 100 mW/cm^2 and dark condition. b) Energy diagram of the electron-only-device.

shows a larger value than that under the dark condition. Moreover, the applied voltage at the minimum current was shifted under illumination, which shift can be obtained in the magnified Fig. 1a. The voltage shift increased because the devices generated the internal voltage, in agreement with the built-in voltage (V_{bi})[26,27], estimated to be 0.6 V of 100 nm Alq_3 devices. The V_{bi} values of the other devices were estimated to be 0.8 V for 150 nm thickness, and 0.2 V for 50 nm thickness of Alq_3. Figure 1b shows the expected energy diagram[20,28,29]. V_{bi} is well-known to correspond with the difference between both the electrodes; however, the polar organic semiconductors have been reported to generate the interfacial charges and the internal voltage, which had affected the work function of the electrodes[30,31]. The V_{bi} values of each Alq_3 thickness were measured to cancel out the Alq_3 effects. These values are required to calculate the injection barrier because V_{bi} exists without illumination. The temperature dependence of the *J-V* curves was measured to estimate the electron injection barrier height. Figure 2 shows the *J-V* curves of the reverse and forward biases at 193–293 K. The applied voltage, i.e., horizontal axis, subtracts the V_{bi} and expresses as an absolute value.

The *J-V* curves of the reverse bias related with the electron injection from the ITO/PEIE/Alq_3 interface (Fig. 2a). The current density increased with increasing applied voltage. Over 7 V, the current density drastically increased; however, it was independent of

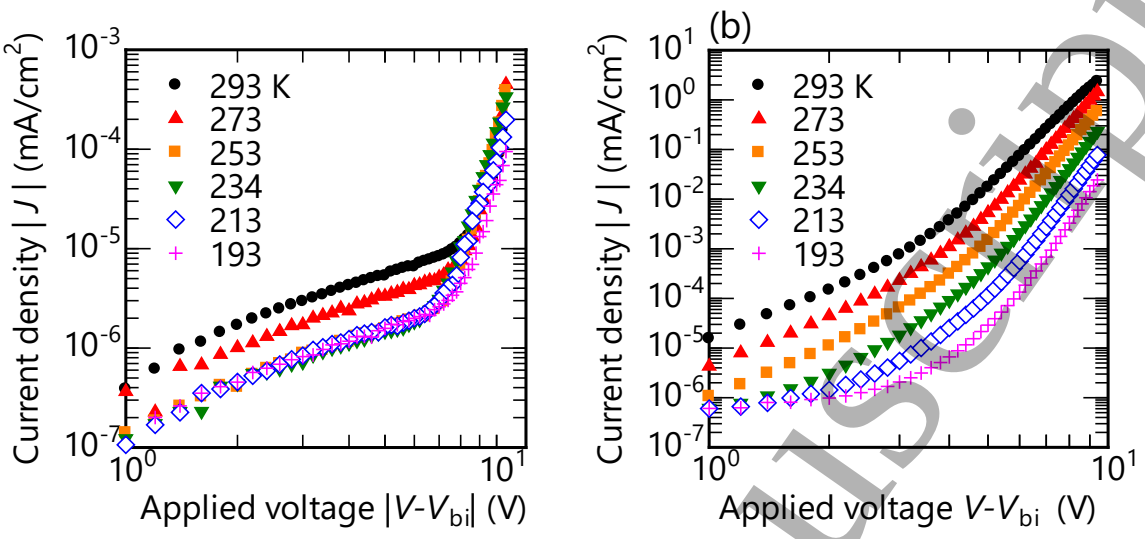

FIG. 2. *J-V* curves of the 100 nm Alq_3 device at 193–293 K,
a) applied the reverse, and b) forward bias voltage subtracted from the built-in voltage.

the measuring temperature. There are two main injection mechanisms for the metal/organic interface—Schottky (thermionic) emission[23,27] and Fowler–Nordheim (F-N) tunneling[32]. The current density in Fig. 2a indicates the tunneling model because of the independence of the temperature. The tunneling current density J_T is given by

$$J_T = \frac{q^3 E^2}{8\pi h \phi_B} \exp\left(\frac{-8\pi\sqrt{2m^*}\phi_B^{1.5}}{3qhE}\right), \quad (1)$$

where q is the electron charge; E is the applied electric field; h is the Planck constant; ϕ_B is the injection barrier height; and m^* is the effective mass, which is equal to the electron rest mass here. Eq. 1 can be re-written as

$$\ln\frac{I}{V^2} = \frac{-8\pi d\sqrt{2m^*}\phi_B^{1.5}}{3qh}\frac{1}{V} + \ln\frac{q^3 S}{8\pi h d^2 \phi_B}, \quad (2)$$

where S is the active area; d is the thickness of the organic layer; and V (= Ed) is the applied voltage. Figure 3 shows the relationship between I/V^2 and $1/V$, given by Eq. 2 because of the simple subtraction of the built-in voltage. The curves of all the thicknesses of Alq_3 are plotted at 193 K because of the low temperature contribution. The F-N tunneling injection model is independent of the measuring temperature; however, the high temperature probably increased the contribution of Schottky (thermionic) emission. Moreover, the large thermal energy could lead to Poole–Frenkel emission in the Alq_3 bulk. To evaluate the tunneling injection model, it was necessary to choose the *J-V* curve with

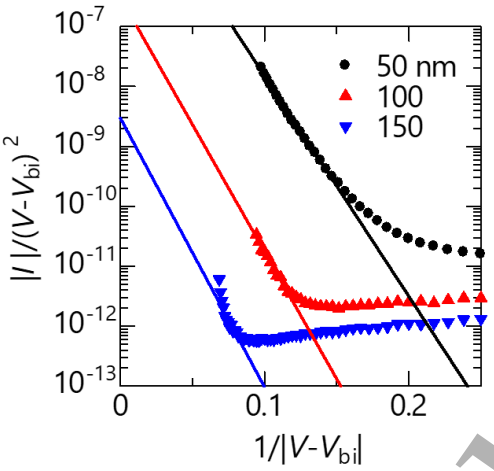

FIG. 3. Relationship between I/V^2 and $1/V$ at applied reverse bias, subtracting the built-in voltage. The slopes of extrapolation yield the tunneling injection barrier height.

the lowest thermal energy. All the curves in Fig. 3 were linearly fitted, provided that the plots of the device breakdown at applying the high voltage were neglected. The slopes of extrapolation led the injection barrier height to be 0.22 eV for 150 nm, 0.27 eV for 100 nm, and 0.40 eV for 50 nm of Alq_3. These values mean the electron injection barrier at the ITO/PEIE/Alq_3 interface, and they decreased with increasing thickness of the Alq_3 layers. This suggests that the high conductivity at the Alq_3 bulk layer decreased the injection barrier. The large current due to the bulk layer was observed with the thick Alq_3 layers, thus promoting the apparent electron injection and leading to the low barrier height.

Subsequently, the *J-V* curves of the forward bias related with the electron injection from the Al/Alq_3 interface (Fig. 2b). The current density increased with an increase in the applied voltage and was dependent on the measurement temperature. This result was different from that of the reverse bias; thus, the injection mechanism at the Al/Alq_3 interface cannot be explained by the F-N tunneling model. The current in Fig. 2b suggests Schottky (thermionic) emission with thermal dependence. The Schottky current J_S is expressed as

$$J_S = A^* T^2 \exp\left(\frac{-q(\phi_B - \sqrt{qV/4\pi\varepsilon_i}}{kT}\right), \quad (3)$$

where A^* is the effective Richardson constant; T is the measurement temperature; ε_i is the dielectric constant of the organic layer; and k is the Boltzmann constant. Figure 4a shows the relationship between J_S and $V^{0.5}$ given by Eq. 3. The low current region is limited by

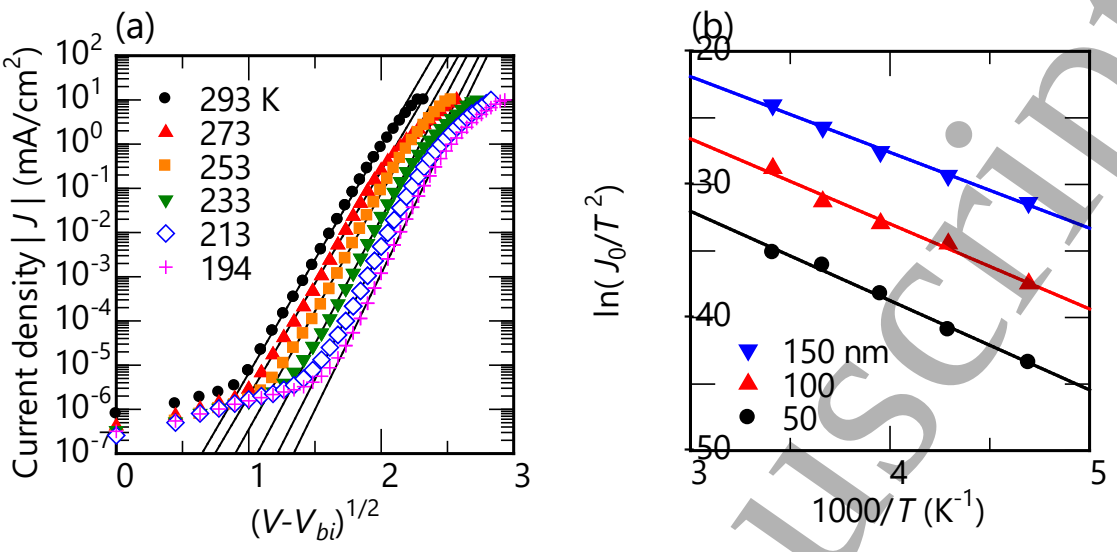

FIG. 4. a) *J-V* curves of the 50 nm Alq_3 device at applied forward bias, subtracting the built-in voltage. The extrapolation gives the current density at zero voltage, J_0. b) The relationship between J_0/T^2 and $1000/T$. The slopes of extrapolation yield the Schottky barrier height.

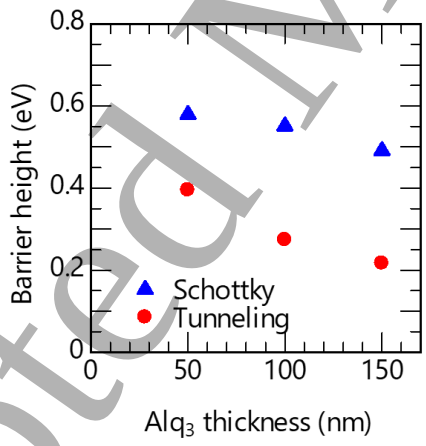

FIG. 5. Alq_3 thickness dependence of Schottky and tunneling injection barrier heights.

the injection from the electrode, and the high current region is limited by the bulk mobility of Alq_3 with sufficient carrier injection. The extrapolation in Fig. 4a led the current density at zero voltage J_0. Eq.3 changes with J_0 to be

$$\ln\left(\frac{J_0}{T^2}\right) = \frac{-q\phi_B}{k}\frac{1}{T} + \ln A^*. \quad (4)$$

Figure 4b shows the relationship between J_0/T^2 and $1000/T$ under different temperatures given by Eq. 4. All plots were fitted linearly; the slope of the extrapolation gave Schottky

barrier heights of 0.49 eV for 150 nm, 0.55 eV for 100 nm, and 0.58 eV for 50 nm of Alq_3. The Schottky injection barrier height decreased with an increase in Alq_3 thickness, as in the F-N tunneling barrier. The estimated barrier heights are summarized in Fig. 5; these values decrease with an increase in the thickness of the organic layer. The bulk conductive current due to the thick Alq_3 layers was superimposed on the measurement current; thus, the apparent low barrier heights were calculated with the enlarged current. The thin organic layer leads to the calculation of the true barrier height because of the low contribution of the bulk conductivity. A lower value for the electron injection barrier height at the ITO/PEIE/Alq_3 interface was observed than that at the Al/Alq_3 interface in this work, and at the metal/Alq_3 interface[23]. Injection to the organic layer from the ITO electrode is generally difficult. Therefore, the results prove that the PEIE layers are beneficial for electron injection from the ITO electrodes. The experimental barrier height values are important for the development of inverted OLED devices.

4. Conclusions

Electron-only devices with PEIE as the electron injection layer were fabricated. These simple devices consisted of ITO/PEIE/Alq_3/Al, and *J-V* curves at 193–293 K were observed. The *J-V* curves applying the reverse bias voltage were independent of the measurement temperature, and those applying the forward bias voltage were dependent on the temperature. In applying the reverse bias, the *J-V* curves can be explained using the F-N tunneling model. The tunneling injection barrier was estimated to be 0.22 eV for 150 nm, 0.27 eV for 100 nm, and 0.40 eV for 50 nm of Alq_3 layer. On the other hand, the *J-V* curves at the forward bias indicated Schottky emission, with the barrier height estimated to be 0.49 eV for 150 nm, 0.51 eV for 100 nm, and 0.57 eV for 50 nm of Alq_3. Both injection barrier heights decreased with an increase in the Alq_3 thickness because the thick bulk layers probably had a contribution of the bulk conductivity and the Pool–Frenkel emission model due to the thermal energy. Therefore, it is required for evaluating the accurate injection barrier to the thin organic semiconductor layer and to the *J-V* curve at the low temperature. A lower value for the tunneling injection barrier heights at the ITO/PEIE/Alq_3 interface in this work were observed than that at the metal/Alq_3 interface; therefore, our results indicate that PEIE is a suitable electron injection material. Thus, we revealed one of

the important physical properties for the development of inverted OLED devices.

Acknowledgments

This work was supported by the Sasakawa Scientific Research Grant from The Japan Science Society, a Charitable Trust of Ame Hisaharu Toyama Prefecture University Research Grant Foundation, and JSPS KAKENHI Grant Number JP19K04465.

Conflicts of interest

The authors declare that they have no conflict of interest.

References

[1] C.W. Tang and S.A. VanSlyke, Appl. Phys. Lett. **51**, 913 (1987).

[2] C.W. Tang, S.A. VanSlyke, and C.H. Chen, J. Appl. Phys. **65**, 3610 (1989).

[3] D. Braun and A.J. Heeger, Appl. Phys. Lett. **58**, 1982 (1991).

[4] L.S. Hung, C.W. Tang, and M.G. Mason, Appl. Phys. Lett. **70**, 152 (1997).

[5] J.T. Lim, C.H. Jeong, M.S. Kim, J.H. Lee, J.W. Bae, and G.Y. Yeom, Jpn. J. Appl. Phys. **46**, 4296 (2007).

[6] M. Sessolo and H.J. Bolink, Adv. Mater. **23**, 1829 (2011).

[7] K. Morii, M. Ishida, T. Takashima, T. Shimoda, Q. Wang, M.K. Nazeeruddin, and M. Grätzel, Appl. Phys. Lett. **89**, 183510 (2006).

[8] H. Fukagawa, K. Morii, M. Hasegawa, Y. Arimoto, T. Kamada, T. Shimizu, and T. Yamamoto, Appl. Phys. Express **7**, 082104 (2014).

[9] T. Makoto, K. Takashi, N. Takashi, and N. Hiroyoshi, Jpn. J. Appl. Phys. **55**, 03DC06 (2016).

[10] H. Kageyama, H. Kajii, Y. Ohmori, and Y. Shirota, Appl. Phys. Express **4**, 4 (2011).

[11] H.J. Bolink, E. Coronado, D. Repetto, and M. Sessolo, Appl. Phys. Lett. **91**, 1 (2007).

[12] M. Takayama, S. Naka, and H. Okada, Jpn. J. Appl. Phys. **52**, 05DC15 (2013).

[13] T. Xiong, F. Wang, X. Qiao, and D. Ma, Appl. Phys. Lett. **93**, 123310 (2008).

[14] Y. Zhou, C. Fuentes-Hernandez, J. Shim, J. Meyer, A.J. Giordano, H. Li, P. Winget, T. Papadopoulos, H. Cheun, J. Kim, M. Fenoll, A. Dindar, W. Haske, E. Najafabadi, T.M. Khan, H. Sojoudi, S. Barlow, S. Graham, J.-L. Bredas, S.R. Marder, A. Kahn, and B.

Kippelen, Science (80-.). **336**, 327 (2012).

[15] X. Qian, L. Song, B. Yu, W. Yang, B. Wang, Y. Hu, and R.K.K. Yuen, Chem. Eng. J. **236**, 233 (2014).

[16] M. Takada, T. Nagase, T. Kobayashi, and H. Naito, Org. Electron. **50**, 290 (2017).

[17] K. SHODA, M. MORIMOTO, S. NAKA, and H. OKADA, IEICE Trans. Electron. **E102.C**, 196 (2019).

[18] A.R. Bin Mohd Yusoff, S.J. Lee, J. Kim, F.K. Shneider, W.J. Da Silva, and J. Jang, ACS Appl. Mater. Interfaces **6**, 13079 (2014).

[19] Y. Wang, L. Zhu, Y. Hu, Z. Deng, Z. Lou, Y. Hou, and F. Teng, Opt. Express **25**, 7719 (2017).

[20] X. Yang, R. Wang, C. Fan, G. Li, Z. Xiong, and G.E. Jabbour, Org. Electron. **15**, 2387 (2014).

[21] S. Höfle, A. Schienle, M. Bruns, U. Lemmer, and A. Colsmann, Adv. Mater. **26**, 2750 (2014).

[22] J. Chen, C. Shi, Q. Fu, F. Zhao, Y. Hu, Y. Feng, and D. Ma, J. Mater. Chem. **22**, 5164 (2012).

[23] S. Naka, M. Tamekawa, T. Terashita, H. Okada, H. Anada, and H. Onnagawa, Synth. Met. **91**, 129 (1997).

[24] K. Banzai, S. Naka, and H. Okada, Jpn. J. Appl. Phys. **54**, 054101 (2015).

[25] Y.-H. Lou, L. Zhang, M.-F. Xu, Z.-K. Wang, S. Naka, H. Okada, and L.-S. Liao, Org. Electron. **15**, 299 (2014).

[26] W. Brütting, S. Berleb, and A.G. Mückl, Org. Electron. **2**, 1 (2001).

[27] M. Matsumura, Y. Jinde, T. Akai, and T. Kimura, Jpn. J. Appl. Phys. **35**, 5735 (1996).

[28] R. Nagata, H. Nakanotani, and C. Adachi, Adv. Mater. **29**, 1604265 (2017).

[29] S.M. Sze and Kwok K. Ng, *Physics of Semiconductor Devices*, 3rd ed. (2007).

[30] Y. Noguchi, Y. Miyazaki, Y. Tanaka, N. Sato, Y. Nakayama, T.D. Schmidt, W. Br?tting, and H. Ishii, J. Appl. Phys. **111**, 114508 (2012).

[31] Y. Noguchi, H. Lim, T. Isoshima, E. Ito, M. Hara, W. Won Chin, J. Wook Han, H. Kinjo, Y. Ozawa, Y. Nakayama, and H. Ishii, Appl. Phys. Lett. **102**, 203306 (2013).

[32] I.D. Parker, J. Appl. Phys. **75**, 1656 (1994).

Figure Captions

FIG. 1. a) *J-V* curves of the 100 nm Alq_3 device under illumination of 100 mW/cm^2 and dark condition. b) Energy diagram of the electron-only-device.

FIG. 2. *J-V* curves of the 100 nm Alq_3 device at 193–293 K,
a) applied the reverse, and b) forward bias voltage subtracted from the built-in voltage.

FIG. 3. Relationship between I/V^2 and $1/V$ at applied reverse bias, subtracting the built-in voltage. The slopes of extrapolation yield the tunneling injection barrier height.

FIG. 4. a) *J-V* curves of the 50 nm Alq_3 device at applied forward bias, subtracting the built-in voltage. The extrapolation gives the current density at zero voltage, J_0. b) The relationship between J_0/T^2 and $1000/T$. The slopes of extrapolation yield the Schottky barrier height.

FIG. 5. Alq_3 thickness dependence of Schottky and tunneling injection barrier heights.